



Article

Google Earth Engine for Large-Scale Flood Mapping Using SAR Data and Impact Assessment on Agriculture and Population of Ganga-Brahmaputra Basin

Arvind Chandra Pandey, Kavita Kaushik  and Bikash Ranjan Parida * 

Department of Geoinformatics, School of Natural Resource Management, Central University of Jharkhand, Ranchi 835222, India; arvind.pandey@cuja.ac.in (A.C.P.); kavita.20260201001@cuja.ac.in (K.K.)

* Correspondence: bikash.parida@cuja.ac.in

Abstract: The Ganga-Brahmaputra basin is highly sensitive to the impacts of climate change and experiences recurrent flooding, which affects large agricultural areas and poses a high risk to the population. The present study is focused on the recent flood disaster in the Ganga-Brahmaputra basin, which mainly affected the regions of Bihar, West Bengal, and Assam in India and neighboring Bangladesh during July, August, and September 2020. Using the Sentinel-1A Synthetic Aperture Radar (SAR) data, the flood extent was derived in the Google Earth Engine (GEE) platform. The composite area under flood inundation for July–September was estimated to be 25,889.1 km² for Bangladesh, followed by Bihar (20,837 km²), West Bengal (17,307.1 km²), and Assam (13,460.1 km²). The Copernicus Global Land Cover dataset was used to extract the affected agricultural area and flood-affected settlement. Floods have caused adverse impacts on agricultural lands and settlements, affecting 23.68–28.47% and 5.66–9.15% of these areas, respectively. The Gridded Population of the World (GPW) population density and Global Human Settlement Layer (GHSL) population dataset were also employed to evaluate flood impacts, which revealed that 23.29 million of the population was affected by floods in the Ganga-Brahmaputra basin. The highest impacts of floods can be seen from the Bihar state, as people reside in the lower valley and near to the riverbank due to their dependency on river water. Similarly, the highest impact was from Bangladesh because of the high population density as well as the settlement density. The study provided a holistic spatial assessment of flood inundation in the region due to the combined impact of the Ganga-Brahmaputra River basin. The identification of highly flood-prone areas with an estimated impact on cropland and build-up will provide necessary information to decision-makers for flood risk reduction, mitigation activities, and management.

Keywords: flood inundation; damage assessment; SAR; GHSL; GEE; TerraClimate



Citation: Pandey, A.C.; Kaushik, K.; Parida, B.R. Google Earth Engine for Large-Scale Flood Mapping Using SAR Data and Impact Assessment on Agriculture and Population of Ganga-Brahmaputra Basin. *Sustainability* **2022**, *14*, 4210. <https://doi.org/10.3390/su14074210>

Academic Editors: Basu Bidroha, Laurence Gill, Francesco Pilla and Srikanta Sannigrahi

Received: 7 February 2022

Accepted: 29 March 2022

Published: 1 April 2022

Publisher's Note: MDPI stays neutral with regard to jurisdictional claims in published maps and institutional affiliations.



Copyright: © 2022 by the authors. Licensee MDPI, Basel, Switzerland. This article is an open access article distributed under the terms and conditions of the Creative Commons Attribution (CC BY) license (<https://creativecommons.org/licenses/by/4.0/>).

1. Introduction

In South Asia, floods have a recurrent occurrence [1], particularly in India where the floods cause an average economic loss of USD 7.5 billion annually [2]. As the frequency of flood events and their severity has increased, the global concerns are also increasing for lessening the fatalities and other economic losses [3]. The flood inundation extent and frequency information are necessary for evaluating the exposure of society, infrastructure loss, economic loss, crop damage, urban flooding [4], flood storage volumes, attenuation of flood waves, and the future flood hazards [5]. In recent times, extreme flood events have intensified riverbank erosion and siltation that has negative impacts on agriculture as well as soil fertility [6]. Flood impacts are also adverse particularly in densely populated regions and compact urban structures. It was estimated that over the last two decades (1995–2015), around 2274 million people were affected by weather-related disasters (i.e., floods, storms) in China, followed by India (805 million), Bangladesh (131 million), and the Philippines (130 million) [7]. Floods alone have affected 2.3 billion people worldwide during 1998–2015

and the majority of those people live in Asia (95%) [7]. About 21 million people worldwide were affected by river floods annually, which may increase to 54 million by 2030 due to climate change and socio-economic growth [8]. The Ganga basin is the most vulnerable area in terms of climate change due to its high population and its high dependency on agriculture [9]. The climate and geology of the Brahmaputra basin have caused many changes to the river channel and bank erosion. The deposition of the sediment load of the Ganga-Brahmaputra delta is the largest in the world and covers an area of 1.76 million km² [10]. Each year, floodings have caused the deposition of the sediment load by 1060 Mt into the Ganga-Brahmaputra delta and Indian Ocean, signifying one of the largest fluvial sediment depositions in the world [11]. Moreover, people living in various regions of the delta often face challenges because of frequent flooding, sea-level rise, cyclone-induced storm surges, and climate change.

Various climatic factors affect floods, mainly through precipitation and including its intensity, amount, and duration. Temperature patterns are also responsible for soil freezing, snow, or ice melt that contributes to a higher amount of runoff [12]. The increasing temperature and the changes in the precipitation intensity or frequency affect the magnitude and the intensity of the floods [13]. The annual mean temperature of the upper Brahmaputra valley region has increased by 0.15° per decade from 1971 to 2007, while rainfall in the summer season has marked a decreasing trend [14]. The study on the seasonal and annual rainfall extent over the Indus, Ganga, and Brahmaputra River basins using the Tropical Rainfall Measuring Mission (TRMM) data of 1998 to 2017 indicated a significant decreasing trend of rainfall in the eastern part of the Indus-Ganga-Brahmaputra (IGB) basins and an increase towards the western part [15]. Increased rainfall has prolonged inundation over land, and some case studies over the Brahmaputra basin area demonstrated that previous floods in 2007 and 2008 have left 1–2 m of the deep sand layer in many villages of Assam in India [6]. A study conducted on the Ganga-Brahmaputra-Meghna basin [16] indicated that the increase in the normal monsoon rainfall and synchronization of flood peaks in the Ganga-Brahmaputra-Meghna basin have caused flooding in Bangladesh in 1988, and such situations can occur more frequently in the Ganga-Brahmaputra plain [17]. All of these result in severe flooding and siltation on the densely populated and agricultural plains of the Ganga and Brahmaputra basin [18].

The rise in temperatures causes a shift in crop growing seasons, which affects food security in many states of India. Due to riverbank erosion, the riverine fertile lands are also reducing, thereby affecting the rural economy of Assam state. The riverbank erosion hazard of the Brahmaputra River has a significant impact on the livelihood of the people, agriculture, environment, and other, different sectors. The continuous loss of output from agriculture and depletion of the ecosystem due to environmental stressors has a major impact on the socio-economic condition of the population [19]. A recent study [20] revealed that the flood of July 2020 has severely affected the cropland of 19,391.42 km² and the settlement of 1509.91 km² in the Indus-Ganga-Brahmaputra basin. Rice and tea yields in the Brahmaputra valley have also been affected by the intra-seasonal variability of both temperature and rainfall distribution during the vegetative phase of the crop [21]. The increasing rate of deforestation and practices of shifting cultivation (Jhoom) [22] in the Himalayan region over the Ganga-Brahmaputra basin has led to various problems including landslides and soil erosion. It subsequently affects the hydrological cycle of the river, producing more rainfall and runoff that results in flooding on the downstream plain area [23]. The study conducted on the impact of soil erosion due to the Brahmaputra River in the Mymensingh district of Bangladesh revealed about 56% of the people lost 0 to 5 acres and 33% lost 6 to 10 acres of their land [24].

The inundation maps help in preventing or reducing flood hazards and risks by providing useful and reliable information to the population [25]. In this context, Remote Sensing (RS)-based data provide multi-resolution satellite data for flood inundation mapping and flood risk zones identification, which are the first steps for the formulation of any flood management strategy [4]. There has been an important contribution of space technology in

the preparedness, prevention, and relief phases of flood disaster management [26]. RS technologies have made it easier to map large areas under flooding and provide early warnings of the disaster [27] that helps in providing support in crisis situations and minimizing damage. Space-based sensors are comparatively more effective than ground-based techniques in providing near-real time data for monitoring the extent of floods [28]. RS analysis can be routinely used to map the flood extent either in near real-time or retrospectively [29]. For the emergency response, it is highly valuable as it offers continued observation about the extent over large geographical areas. For the effective production of flood inundation maps, the selection of suitable sensors is a major challenge [30]. The satellite platforms and other advances in RS have provided a wide range of applications of satellite data. Several studies have utilized optical satellite data and related flood products (e.g., MODIS-based NRT) to monitor and assess flood impacts across several river basins [27,31–33].

Moreover, it is a fact that the optical sensors data has an inherent problem in flood studies [34]. Therefore, several researchers emphasized the utility of Synthetic Aperture Radar (SAR) data for flood studies. SAR sensors can easily penetrate clouds and severe rains conditions during flood and post-flood events. SAR data are therefore preferred in real-time flood damage assessment as they discriminate land and water precisely [35]. However, the limitation of the SAR sensor is its revisit period (e.g., 12–24 days), which results in less availability of SAR images during flood seasons. For instance, in the Ghaghara River, which is a major left bank tributary of Ganga, high-resolution multi-temporal SAR data was used to find the flood inundated area due to the rise in the water level of the river. It concluded that the results obtained by the SAR data can be used effectively for flood mapping and monitoring [36]. The SAR data was used during August–September 2018 to map severe flood conditions and explained the impact of flooding over the Ramganga River in the Ganga basin. It also revealed a severe bank erosion that took place in the channel with an average increase in the width of the channel from 46 m to 336 m [37]. In the year 2019, the flood situation in severely affected Bihar was assessed using Sentinel-1 SAR data (C-band) and ground-based gauge data, along with other variables (i.e., precipitation, soil moisture, vegetation cover) [6]. It revealed that the Ganga River was flowing above the danger level for two weeks and prolonged flood inundation led to severe damage to the vegetation and population [6]. The SAR data and Digital Elevation Model (DEM) have been used effectively for mapping flood extent and flood depth in the Kosi River basin in the North Bihar region [38,39]. SAR-based flood prognosis analysis leads to spatial accuracy and can be even improved when coupled with hydrological models or other hydro-meteorological parameters [40]. Sentinel-1 SAR-based flood inundation maps have provided an accuracy of 96.44% in Bangladesh [41]. The open-access Sentinel-1 data with geospatial techniques have been widely used and provide an immediate assessment for the flood disaster. Google Earth Engine (GEE) has been widely used for better and faster data processing and analysis of results. GEE is a cloud-based platform for geospatial analysis. It is an integrated platform designed to empower a wide audience, including remote sensing scientists lacking the technical knowledge of supercomputers [42]. The GEE environment makes it easier for managing data, allocating resources, data distribution, and large computations by utilizing parallel processing.

The Ganga-Brahmaputra basin is affected by flooding on a recurrent basis and the pattern of occurrence of flooding has been changing with the increasing impacts on agriculture, settlements, and the population due to climate change. The objective of the study is (1) to monitor the large-scale flooding in 2020 in the Ganga-Brahmaputra basin using SAR data in cloud platform GEE, and (2) to estimate the impact of floods on the agriculture and population in the basin. The analysis of the spatiotemporal distribution of flooding in the Ganga-Brahmaputra basin will provide useful insights into the formulation of disaster risk maps, mitigation measures, and emergency management.

2. Study Area

The study area comprises the Ganga-Brahmaputra basin that lies in the subtropical regions situated between 10° N to 30° N latitude and 84° E to 95.5° E longitude (Figure 1). The states situated in the basin comprise Assam, Bihar, and West Bengal in India, as well as Bangladesh. The basin is formed as a result of the many tributaries from the Ganga and Brahmaputra River. Some of the tributaries of the Ganga joining the basin are the Ghaghra, the Son, the Gandhak, the Chambal, and the Kosi. The tributaries of the Brahmaputra joining the basin are Teesta and Meghna. This basin covers a very large area and is spread over different countries including India, China, Nepal, Bhutan, and Bangladesh. The main features of the Ganga-Brahmaputra basin are the fertile land, the Himalayas, and the delta of the Sunderban. The major area of the Ganga basin falls within the 300–500 m elevation zone, whilst the floodplain of the Brahmaputra basin falls within 100 m. This basin receives heavy showers in the monsoon season during the period from June to September, which accounts for about 80% of the annual rainfall. The demography of the entire basin is affected by various factors with mountain regions exhibiting a lower population compared to the fertile plain areas. The basin comprises the homes of almost 625 million people, out of which 80% are farmers and are dependent on the water from the river for carrying out agriculture activities. Bangladesh gets most of its water (94%) from the river flowing through the country. In Assam, recurrent floods affected about 1846 villages and 1.6 million people during the 2014 flood event, whereas in the 2016 floods, nearly 2893 villages and 1.7 million people were displaced [43]. The historical major flood events in Assam, Bihar, West Bengal, and Bangladesh have been shown in Table 1.

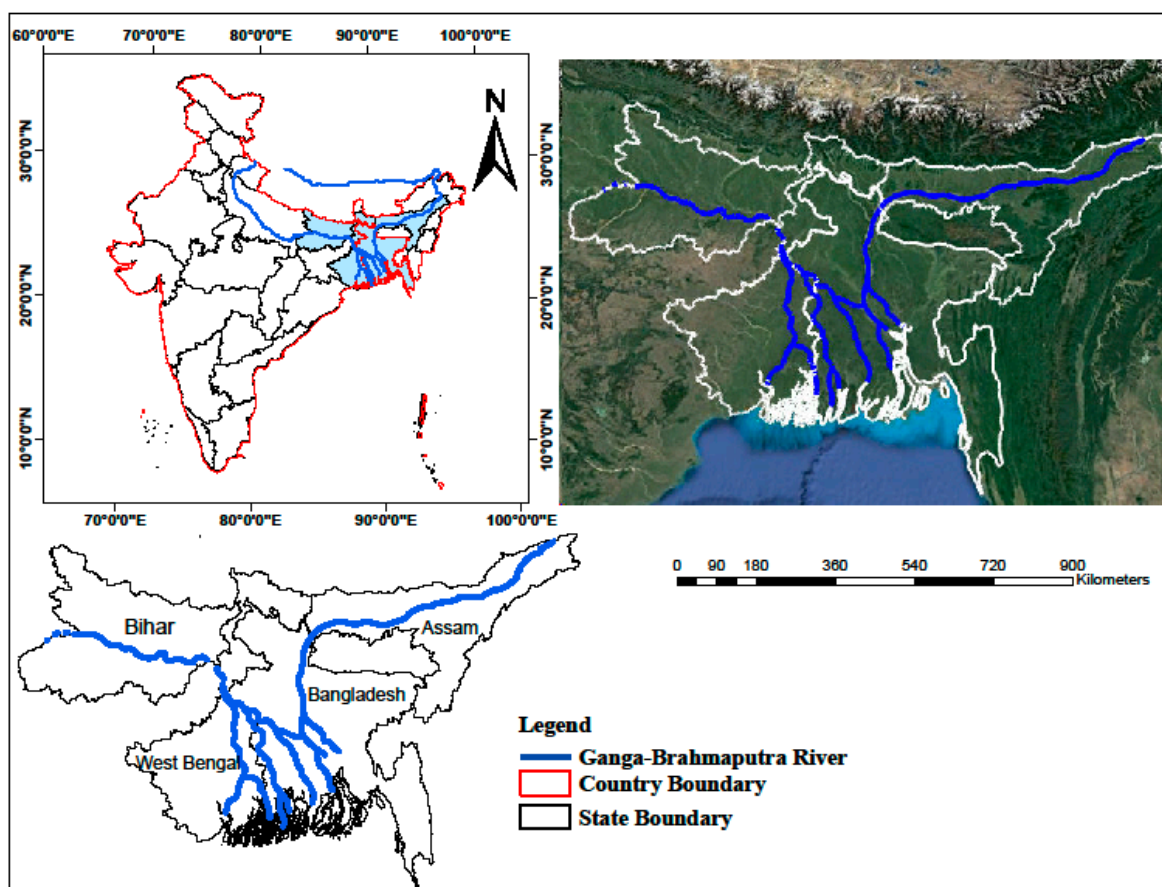


Figure 1. Study area Ganga-Brahmaputra basin.

Table 1. Past flood events in the Ganga-Brahmaputra basin.

States/Country	Flood Events	Source
Assam	1954, 1962, 1966, 1972, 1974, 1977, 1978, 1983, 1984, 1988, 1998, 2000, 2002, 2004, 2012, 2013, 2015, 2016, 2017, 2018, 2019, 2020, 2021	[44]
Bihar	1987, 1995, 1998, 2000, 2001, 2003, 2004, 2008, 2010, 2013, 2016, 2017, 2018, 2019, 2020, 2021	[31,40]
West Bengal	1913, 1942, 1954, 1965, 1956, 1959, 1978, 1993, 1995, 1999, 2000, 2001, 2002, 2005, 2006, 2010, 2012, 2013, 2014, 2016, 2018, 2019, 2020, 2021	[45]
Bangladesh	1842, 1858, 1871, 1875, 1885, 1892, 1948, 1953, 1954, 1955, 1956, 1962, 1963, 1968, 1970, 1971, 1974, 1984, 1987, 1988, 1993, 1995, 1998, 1999, 2004, 2006, 2007, 2010, 2011, 2014, 2015, 2017, 2019, 2020, 2021	[46]

3. Materials and Methods

Data Used

The present study used primarily Sentinel-1 SAR data for flood inundation mapping in 2020 in the Ganga-Brahmaputra basin. The flood damage assessment has been performed using land use land cover (LULC) as well as a population dataset. The detailed data used, as well as the sensor characteristics, have been given in Table 2. The Copernicus Global land cover dataset was acquired from the European Space Agency (ESA) to extract the cropland and build-up in the Ganga-Brahmaputra basin for damage assessment, whereas the population density was used to evaluate the affected population and identify density areas within closer proximities of the river. The Global Human Settlement Layers (GHSLs) and Gridded Population of the World (GPW v4) datasets on the population and population density, respectively, were employed to evaluate flood impacts. The Terra Climate monthly precipitation data were used to observe the rainfall pattern and rainfall anomaly for the flood event in 2020. The agricultural area and population density were extracted using ArcGIS software. Shapefiles of the country, state, district, and the river were used to separate the entire study area and to get the flood impact area statistics at different levels. For the validation of flooding extent, the Operational Land Imager (OLI) of Landsat-8 satellite images were used.

Table 2. Data used and their specifications.

Dataset Used	Spatial/Temporal Resolution	Acquisition Date	Purpose	Source
Sentinel-1A (SAR)	10 m, 12 days	July–September (2020) March 2020	Flood extent mapping Pre-flood images	ESA
Landsat-8 (OLI)	30 m, 16 days	March 2020 July–September (2020)	Pre-flood images during-flood images for validation	Earth Explorer
TerraClimate: Rainfall	4 km, monthly	July–September (1990–2020)	Rainfall distribution Rainfall anomaly	[47]
GHSLs: population	9 arcsec	2015	Affected population	[48]
GPW v4: population density	1 km	2020	Population density	[49]
Copernicus global Land Cover	100 m	2019	Affected LULC extraction	[50]

The constellation of Sentinel-1A and Sentinel-1B are on a sun-synchronous, near-polar orbit. The Ground Range Detected (GRD) product of the Sentinel-1A satellite provided data in the C-band dual-polarization channels (VH and VV) with a repeat cycle of 12 days and was used to extract the flood inundated area. The pixel spacing resolution of the Sentinel-1A data is 10 m. The SAR images were processed directly in GEE from July to September in 2020 and, furthermore, used for identifying flood pixels. TerraClimate data provide many climatic variables at ~4 km spatial resolution at monthly time scales. In the present study, the spatial pattern of the rainfall for July to September 2020 was derived from this dataset, whilst the rainfall anomaly for 2020 was computed using the long-term mean over 1990 to 2019.

The global human settlement and population product were available at 9 arcsec and 30 arcsec, respectively. Then, rasterization in the final grids was performed by adding point values per pixel. This raster product depicts the distribution of the population and its density expressed as the number of people per cell. The GPW (v4) was adjusted to the 2015 revision of UN World Population Prospects (WPP) country totals [51]. It consists of the estimates of the population density (i.e., expressed as number of persons per km²) based on the counts, which are consistent with censuses and population registers. Nearly 13.5 million administrative units of national and sub-national are utilized and were used to assign adjusted population counts to 30 arc-second grid cells. The density raster data is calculated by dividing the UN WPP adjusted population count data for any given year by the land area raster.

The Copernicus 100 m Global Land Cover data are yearly moderate resolution maps that are updated annually and are freely available [50]. The Copernicus LULC data were mapped with high temporal stability across time and have an overall accuracy of over 80%.

4. Methodology

Sentinel-1A SAR data was used to generate the flood extent map based on a change detection approach (CD) where a before-flood image and a during-flood image were compared. The pre-processing techniques used before the generation of the map were thermal noise removal, radiometric calibration, speckle filter, and terrain correction (Figure 2). The GEE platform is used for performing all pre-processing steps (Figure A1). A speckle filter with a smoothing radius of 50 m was applied during the processing to reduce the effect of the granular noise. The terrain correction is applied to rectify the geometric distortions inherent in SAR images. To estimate the changes due to flooding, the during-flood mosaics were divided by the before-flood mosaics using a threshold of 1.25. In the resultant image, the brighter pixels with higher values exhibit large changes as compared to the darker pixels (low values). Then, the binary raster layer is created with the threshold value of 1.25, assigning 1 to all the values greater than 1.25 (flood pixels) and 0 to all values less than 1.25 (non-flood pixels). The 'VH' polarization was preferred for flood mapping because of the overestimation of results obtained through 'VV' polarization. VV polarization is susceptible to vertical structures, whereas VH polarization is more sensitive to the changes on the land surface. VH polarization is more suitable for determining the flood-affected areas as it manifests higher dark and black tones as compared to VV polarization [51,52]. After the flood inundation extent was derived, the permanent water bodies (PWB) were removed from the result using the Copernicus 100 m LULC product and the clipping tool in ArcGIS. The rainfall anomaly was created for monsoon season 2020 (July to September) by taking the average rainfall over the months with respect to the long-term 30-year mean rainfall (1990–2019) from July to September. The rainfall distribution and rainfall anomaly were shown to link with the flooding extent in the study area as higher intensity rainfall in upstream areas caused heavy riverine flooding in the downstream areas.

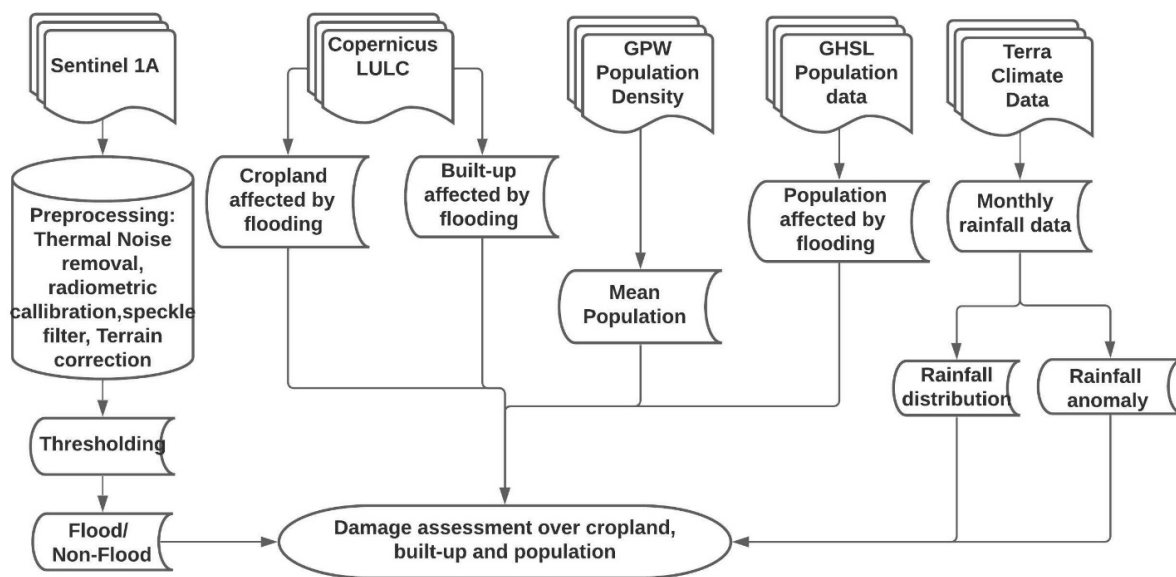


Figure 2. Methodology adopted to assess flood and its impact assessment over agriculture, built-up, and population density.

For agriculture area extraction for the entire study area, the Copernicus Global Land Cover product was used. To extract the cropland, the LULC raster data was firstly converted to a vector format and classes containing the same values for the cropland were merged together. Furthermore, the pixels of the cropland overlapping with the flood inundation extent were extracted using the clipping tool to estimate the percentage of the cropland area affected from the total inundated area. The same process was used to extract the built-up area affected due to flooding. The population density was calculated for the entire region using the GPW v4 population density data. To identify the population affected by the flood in the areas nearby the rivers, the GHSLs population data were used with the inundated extent. The assessment of the damage from the floods over the agriculture area and the population was carried out using flood inundation during August, September, and October 2020. The detailed methodology has been shown in Figure 2. The LULC raster data collected from Copernicus was resampled to a 10 m spatial resolution using the nearest neighborhood method for comparison and overlaying with the flood map. Similarly, the GHSLs and GPW data were resampled to a 10 m spatial resolution for deriving the population affected by the flooding and population density.

5. Results

5.1. Rainfall Distribution and Anomaly during 2020 Flood Event (July to September)

The rainfall pattern and rainfall anomaly from July to September (monsoon season) for the year 2020 have been shown in Figure 3. The rainfall pattern showed that the higher rainfall intensity was confined to the parts of Meghalaya, which were observed as more than 800 mm. The intensity of 600–800 mm was observed in parts of Sikkim and the upper reaches of West Bengal. The overall intensity of the study area was observed between 200–400 mm. Whereas the upstream areas of the Ganga-Brahmaputra basin, like parts of Nepal, Arunachal Pradesh, and Nagaland, have contributed a higher rainfall than the downstream areas (Figure 3a), which have resulted in excessive flooding conditions in the lower Ganga-Brahmaputra valley. Similarly, the highest rainfall anomaly during July to September 2020 exhibited that the maximum anomaly (200–400 mm) was noticed in the upstream areas of the Ganga-Brahmaputra basin. Moreover, several parts of the Ganga-Brahmaputra basin also exhibited positive rainfall anomalies between 50–200 mm (Figure 3b), albeit some parts of the study regions in the downstream area (i.e., Assam and Bangladesh) have shown negative rainfall anomalies (50–100 mm).

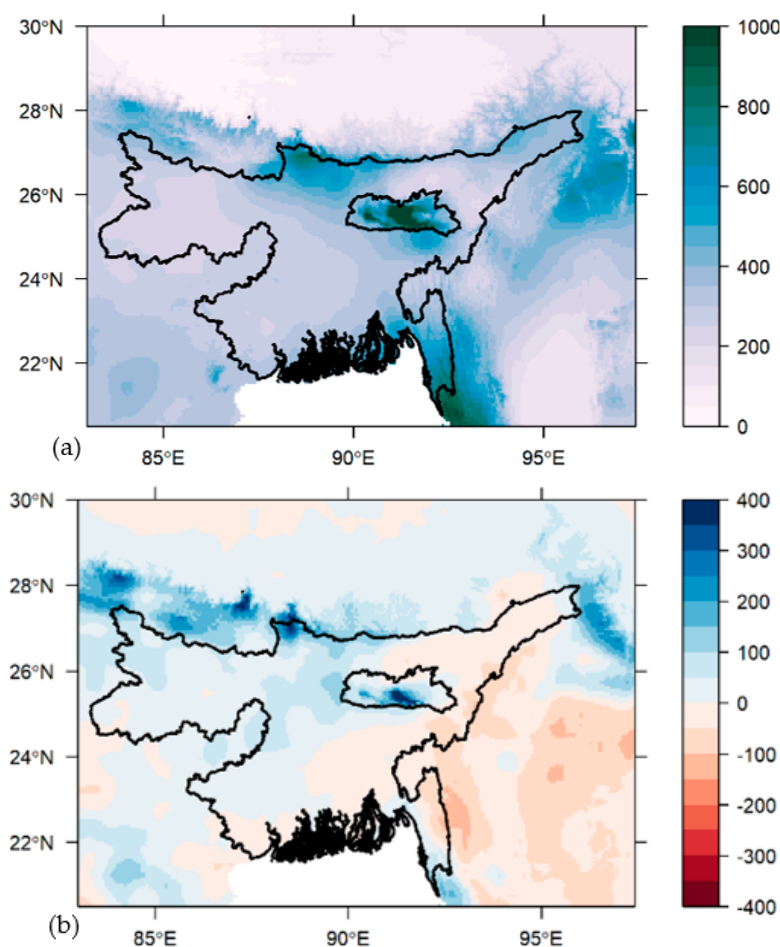


Figure 3. Rainfall distribution (a) and anomaly (b) in mm during July–September 2020. The rainfall anomaly was derived from the long-term 30-year mean (1990–2019).

5.2. Flood Extent in 2020 as Derived from SAR Data

The inundation extent acquired from the Sentinel-1A data showed a continuous regression of flooding from July to September 2020 (Figure 4). The flood inundation affected a large extent of area with a significant impact in Assam, Bihar, West Bengal, and Bangladesh in July (Figure 4a). However, the flood inundation extent reduced in subsequent months, like August and September, indicating flood regression (Figure 4b,c). The excessive flooding area was the result of excessive rainfall in the upstream areas of the Ganga-Brahmaputra basin with rainfall more than 600 mm. In Assam, the flood extent was largely confined to the proximity areas of the Brahmaputra River, whereas for Bihar, the tributaries of the Ganga constitute the major zones of flood inundation due to breaching along the banks of the tributary rivers owing to the excessive rainfall throughout the monsoon season. The accumulated river flows from the Ganga and Brahmaputra rivers lead to excessive floods in Bangladesh along the river Meghna. A major zone of flood inundation was also noticed in the downslope areas just south of the Meghalaya Plateau region where flows from the plateau region get accumulated in the plain region resulting in severe flood damage in two different zones in Bangladesh. The region-wise affected areas were shown in Table 3 for July, August, and September 2020. The flood extent was highest in July in all four regions, whereas lowest in September. As per the composite flood inundation, it was found that 17.16%, 22.11%, and 20.31% of the area was affected in Assam, Bihar, and West Bengal, respectively. In the case of Bangladesh, 18.51% of the area was inundated during the monsoon season in 2020. Overall, floods have inundated 19.48% (77,493.1 km²) of the areas in the Ganga-Brahmaputra basin.

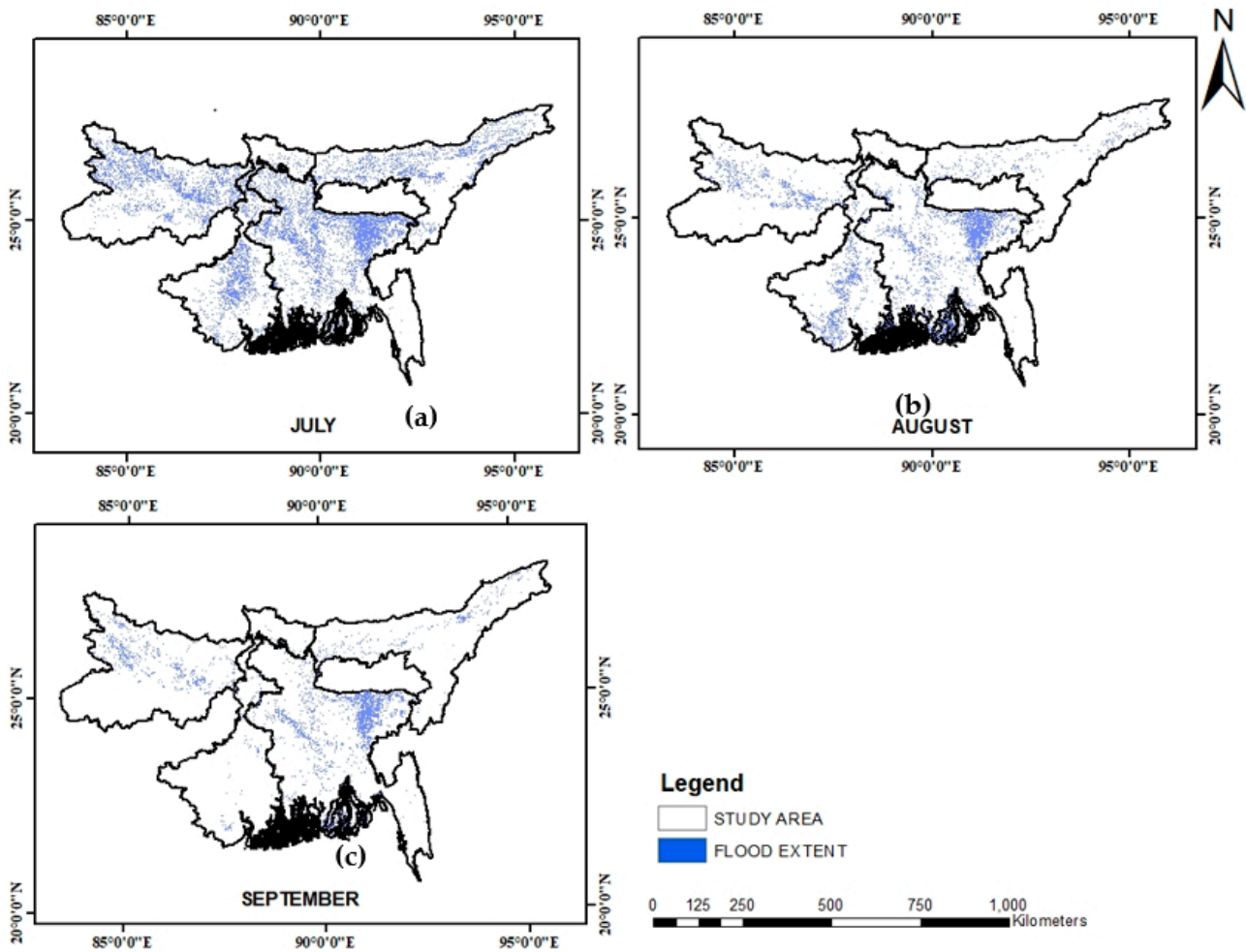


Figure 4. Flood extent during the time period of July (a), August (b), and September (c), 2020, respectively.

Table 3. Flood inundation extent (km²) in Assam, Bihar, West Bengal, and Bangladesh. The % area in the last column was calculated with respect to irrespective total area of the states.

Study Area	Total Area (km ²)	Inundated Area (km ²)			Composite Area (km ²) (%)
		July	August	September	
Assam	78,431.2	12,173.5	4215.54	3007.10	13,460.1 (17.16%)
Bihar	94,234.6	18,424.8	8679.91	5025.71	20,837 (22.11%)
West Bengal	85,194.9	12,917.5	9368.75	1439.34	17,307 (20.31%)
Bangladesh	139,846	30,734.47	21,569.4	15,615.42	25,889 (18.51%)
Total	397,706.7	74,250.27 (18.67%)	43,833.6 (11%)	25,087.57 (6.3%)	77,493.1 (19.48%)

5.3. Flood Inundation Impact on Cropland and Settlement

The flood impact on LULC was analyzed using the Copernicus Global Land Cover data with a 100 m spatial resolution. The spatial pattern showed that the croplands and build-up were adversely affected by the floods (Figure 5). The area statistics of the croplands and build-up affected by the floods were presented in Table 4. In Assam, 28.47% and 9.15% of the croplands and build-up areas, respectively, were affected by 2020 flood events, whereas in Bihar 24.54% and 7.29% of the areas of croplands and build-up were affected. In West Bengal, 24.63% of the cropland and 5.66% of the built-up areas were

affected, whereas in Bangladesh, 23.68% and 5.8% of the areas of cropland and build-up were affected, respectively.

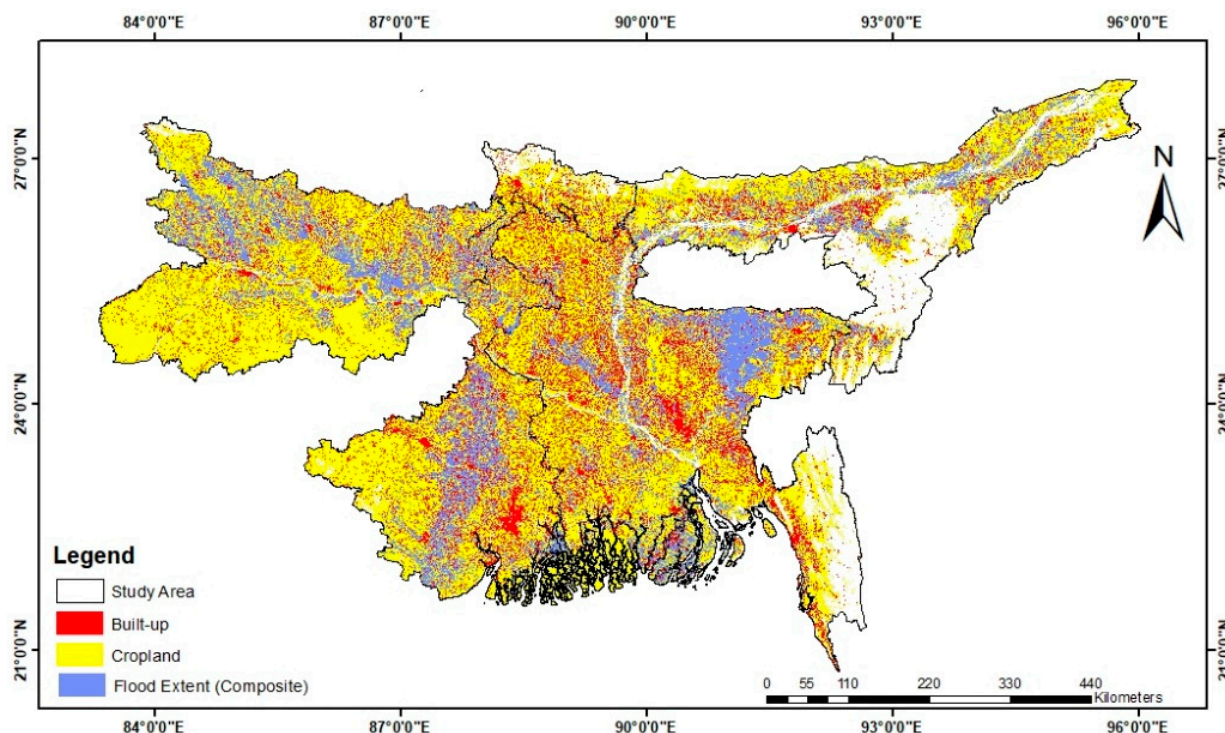


Figure 5. Flood inundation as derived from composite maps (July–September) and its impacts on LULC.

Table 4. Flood impacts on croplands and built-up as derived based on the composite flood map. Others indicate the LULC classes other than croplands and built-up.

States	Total Cropland (km ²)	Affected Cropland (km ²) (%)	Total Built-Up (km ²)	Affected Built-Up (km ²) (%)	Affected under Others (km ²)
Assam	43,678.78	12,439.56 (28.47%)	8213.44	751.86 (9.15%)	268.68
Bihar	81,112.49	19,911.18 (24.54%)	10,908.93	796.01 (7.29%)	129.81
West Bengal	64,823.88	15,969.33 (24.63%)	15,049.51	852.1 (5.66%)	485.57
Bangladesh	95,468.85	22,614 (23.68%)	27,734.92	1610.75 (5.80%)	1664.25

5.4. Flood Inundation Impact on Population

The mean population of the study area represents a high density of the population that is mainly in the flood plain areas along the major rivers (Figure 6). The mean population values are highest for Bangladesh, ranging from 0 to 1249.37 per km²; followed by West Bengal with the mean population value of 1216.55 per km²; Bihar with 1357.65 per km²; and Assam with 455.80 per km². The population of Bangladesh is at higher risk as compared to other states of India given that it comprises the confluence zone for the Ganga-Brahmaputra River and is a low-lying area with the highest density in the world, which makes its population more prone to flood risk. After applying the zonal statistics on the GHSL population data of the year 2015, the total population was extracted and was estimated as 33.50 million in Assam, 115.92 million in Bihar, 97.13 million in West Bengal and 160.10 million in Bangladesh. As per the GPW dataset, a population density of 110,425 persons per grid was found in Bangladesh, which co-located with the inundated area during the peak flood period and was followed by Bihar and Assam in India with 48,409 and

46,943 persons per grid, respectively, whereas the least was in West Bengal with only 3092 persons per grid.

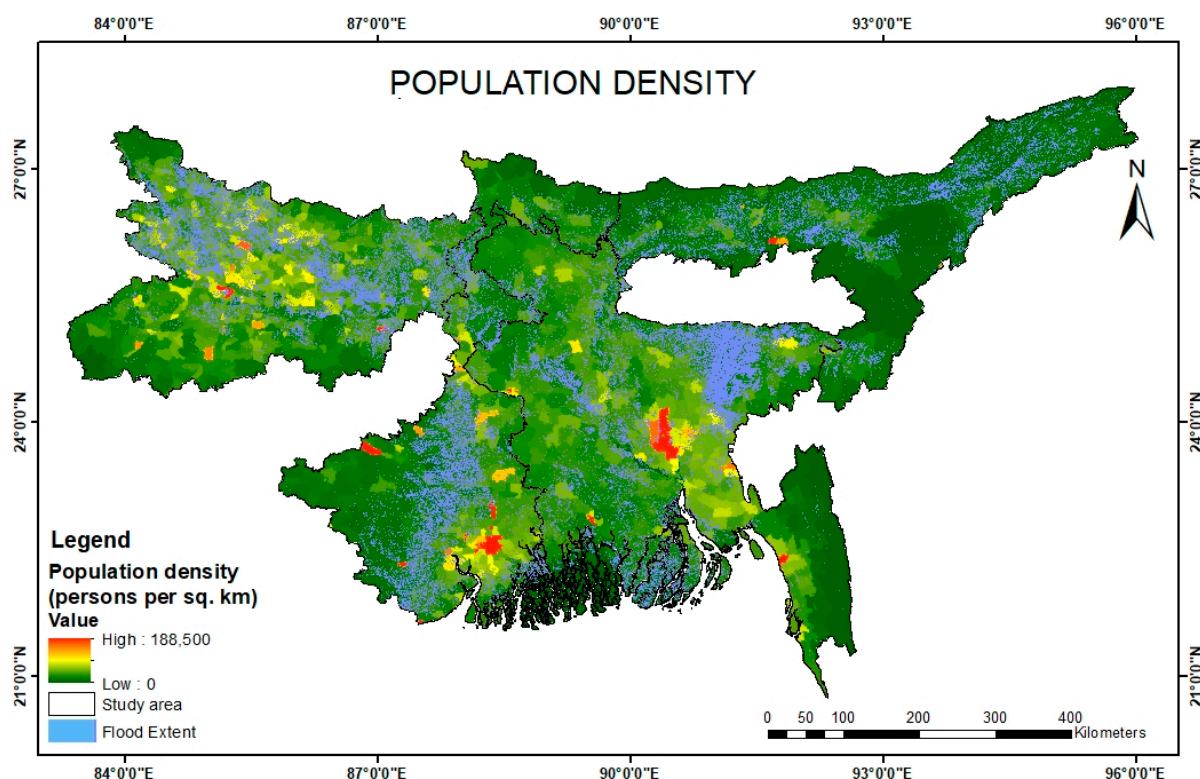


Figure 6. Mean population per km² of the study area.

The estimation of the population is necessary for the analysis of the severity of the flood hazard. There is a higher concentration of the population in the lower valley regions in Assam due to the population's dependency on the river water, but the density of the population is still very low as compared to other states included in the study area. A large population was flood-affected in Bihar due to the presence of a number of tributary streams in the higher population density region. The population affected by the floods was higher in the month of July and urban areas experienced the most impacts and damage due to the extensive rainfall that led to the floods. The affected population due to flooding impacts was shown in Table 5. Bihar was the most affected among others with an affected population of 11.79 million, followed by Bangladesh (6.9 million), Assam (3.2 million), and West Bengal (1.4 million). In August, the highest impact was found in Bihar with 7.6 million persons affected, followed by Bangladesh (5.6 million), West Bengal (1.9 million), and Assam (1 million).

Table 5. Flood impacts on population as derived based on the composite flood map.

Study Area	Total Population	Affected Population
Assam	33.50 million	3.2 million
Bihar	115.92 million	11.79 million
West Bengal	97.13 million	1.4 million
Bangladesh	160.10 million	6.9 million

6. Discussion

The Ganga-Brahmaputra basin is highly prone to flooding because of extensive rainfall events that occur over a shorter time span, which is influenced by climate change. Among hydrometeorological hazards, flood occurrences and magnitude are increasing in recent decades because of global climate change [53,54]. Studies have found that temperature trends have been increasing in South Asia [55]. Similarly, monsoon precipitation patterns have been altered especially in the Ganga-Brahmaputra delta, with an indication of increased risk of flooding in the monsoon season as suggested by Regional Climate Model (RCM) simulations [55,56]. The impact of climate change on the water resources of the snow and glacier-dominated river basins is also important for water resource management. The river discharge in the Brahmaputra river is highly influenced by the snowmelt at the upper part of the catchment due to global warming [57]. The snow cover area changes under the recent climatic conditions are expected to have a larger effect on the hydrological cycle [58]. Satellite gravimetry was used to understand the contribution of substantial meltwater to the Brahmaputra river and found that summer meltwater contributed 43 ± 8 Gt to the Brahmaputra. There is a high sensitivity between glacier and snow melting with temperature on annual, as well as monthly scales, suggesting changes in the total annual discharge as well as an earlier peak of runoff due to global warming [59]. Furthermore, the Ganges-Brahmaputra delta is known to be the most vulnerable to the effects of climate change, mainly due to anthropogenic stressors as well as the larger population.

During and after the disaster, remotely available data is beneficial for rescue work and restoration. For the purpose of disaster risk management, satellite data can play a powerful role by helping to identify the major extent of flooding and its impacts on croplands, build-up, and the urban population, and, based on this information, relief work can be started on an emergency basis. Satellite data also provides instant flood situations with greater accuracy. Unfortunately, optical satellite data are not available during the time of disaster (especially floods) for analysis due to the excessive cloud cover. Whereas Sentinel-1A (SAR) data is beneficial for flood monitoring during and after any flood event because of the availability of its data during day and night with no impact on cloud cover.

The pattern of rainfall intensity and rainfall anomaly during July to September 2020 was analyzed using the TerraClimate data. The rainfall anomaly has shown a positive pattern (200–400 mm) in the central parts of Bihar, Assam, West Bengal, and Bangladesh—except for certain parts of Assam in the northeastern states of India. It was observed that the upper reaches of the Ganga-Brahmaputra basin led to the excessive flow of floodwater in the lower elevation areas of Bihar, Assam, West Bengal, and Bangladesh. Especially for Bangladesh, the upper parts of excess rainfall states like Meghalaya, Arunachal, and Assam altogether contribute to huge damage to the country and its economy, which is due to recurring floods. The areas surrounding the river body of either the Ganga or Brahmaputra are highly populated because the Basin region is an important agricultural belt of the country. Bihar is highly influenced by the various stream systems and the flow of river water from the Himalayan region [60], thereby creating havoc for the state during every monsoon season [61]. Most of the inundated area was confined to the North Bihar region. Based on the Sentinel-1A (SAR) data, the present study estimated that the total inundation during July was about $74,250.27 \text{ km}^2$ (18.66%) with a regression in August resulting in $43,833.6 \text{ km}^2$ (11%) and in September, which resulted in $25,087.57 \text{ km}^2$ (6.3%). As per the composite flood maps during the 2020 flood events, it inundated 19.48% ($77,493.1 \text{ km}^2$) of the areas in the Ganga-Brahmaputra basin with a maximum inundation in Bihar (22.11%), followed by West Bengal (20.31%), Bangladesh (18.51%), and Assam (17.16%). The SAR-derived flood map was validated against the false color composite (FCC) images of the optical data (Landsat-8) acquired during the same time period as the SAR data (Figures A2 and A3), albeit some of them are cloudy images. These results show that the flood extent map was accurate to that seen in the optical FCC images as well as the grey-color images of the SAR data (Figures A2 and A3). Moreover, these results are consistent with the latest study, which has reported based on the MODIS NRT flood product that about

17.7% of the geographical area of North Bihar was inundated during 2020 flood events and the adversely affected districts were Muzzafarpur, Darbhanga, Saharsa, Khagaria, Madhepura, Bhagalpur, Katihar, and Purnea [62]. Previously, during the flood event of August–September 2017, 12% to 17% of the geographical area of North Bihar was inundated during the peak flood period [57]. The composite floods maps over 2000–2020 indicated that about 34% of the area was affected by floods, as derived from the MODIS-based NRT flood product [57]. In Assam, our estimates on the flood inundation area and the spatial pattern were very consistent with Devrani et al. [63], who have reported an inundation of 14,445.28 km² (18.42%) based on the Sentinel-1 SAR data. During the floods of 2017 in Bangladesh, the maximum damage was observed in August with an inundated area of about 7.01% of the total geographical area of Bangladesh [41], and the flood-related inundation mostly varied from 20–25% [12]. The different hydrological models were used mainly to derive the peak discharge changes, volume of the flood, and the annual water yield [64]. The extent of the floods from these flood inundation models was validated with the help of ground truth surveys, which were not a very reliable source [65] on account of the limited field observations. Hence, by utilizing the SAR-based data and processing these data in a cloud platform like GEE, it proved to be an efficient technology to provide near real-time monitoring and management of flooding situations on any geographical setup.

Several tributaries and distributaries of the Ganga affect a vast area of Bihar, damaging the cropland and build-up. The major built-up areas of the study are mostly confined to the river channel due to the availability of freshwater, resulting in higher damage to the infrastructure. Major damage to the croplands was found in the Ganga-Brahmaputra basin as most of its area was under cultivation during the monsoon season. The present study showed that the floods in 2020 have affected the croplands area between 23.68% (Bangladesh) to 28.47% (Assam) and the built-up area between 5.66% (West Bengal) to 9.15% (Assam). Most of these results are in line with previous studies that have reported the impact of floodwater on agricultural land and urban areas, especially in Bihar [34,62]. The flood impacts in North Bihar during the 2017 flood events were the highest in agriculture (19%), followed by the forest (0.58%) and built-up classes (0.4%) [42]. The flood impacts on croplands in Bangladesh during the 2017 flood event were 1.51% in April, 3.46% in June, and 5.30% in August [63], which was much lower than the impacts observed in the 2020 flood event. The maximum damage to the build-up was found in Assam (9.15%) and Bihar (7.29%) in comparison to West Bengal and Bangladesh, since most of its population resides in the lower valley near the river that affected 11.79 million of the population in Bihar and 3.2 million of the population in Assam. In Assam, the population residing in the valley region is adversely affected by the high flow of the Brahmaputra River. The upper part of West Bengal and Bangladesh also receives higher flows from the Himalayan region, which affected a population of 6.9 million and 1.4 million, respectively—although it was comparatively lower than Bihar.

In terms of population, the region is highly vulnerable as the study area incorporates the highest density regions of the world. Most of the affected population constitutes the lower-income groups of the states that are forced to stay in spite of the disastrous impact of floods. The GPW v4 is a good source that provides high resolution population densities of the world. The population density is highest in Bangladesh, including Bihar and West Bengal, as compared to the world and, therefore, the highest densities make these countries the most vulnerable population to frequent occurring disasters. As derived from this dataset, it can be concluded that the study area is under a high disaster risk zone and major and early steps are required to control the impacts of floods on the livelihood and economic condition of people. This paper will help identify the flood-affected zones and the areas that should be taken into consideration to minimize the impact of naturally occurring disasters. Natural disasters cannot be controlled and, therefore, their impact on croplands and build-up can be minimized. GHSLs provide population density and count data that can be used for the estimation of the flood-affected population. Global population grids are used for various applications for analysis, modelling, and policymaking [66].

The estimation of the population is necessary for defining the severity of flood exposure. Resources are the root cause that limits the locational choices of the vulnerable groups in avoiding hazardous areas [67]. The higher exposure of socially vulnerable groups can lead to a greater susceptibility to impacts during flood disasters [68].

Notably, it is worth mentioning that accurate and high resolution LULC datasets are important for damage assessment. However, there are some inconsistencies in the LULC classes in different products, which makes it difficult to perform damage assessment of LULC classes due to flooding. For instance, the built-up class in the MODIS-based LULC dataset is underestimated, whereas the ESRI LULC dataset, as prepared from Sentinel-2 (10 m resolution), has been overestimated. In this context, we find that the Copernicus LULC dataset of ESA was beneficial for deriving the damage to both the cropland and built-up, albeit the latter one is still overestimated. Though the ESRI LULC dataset is available at high resolution, the only setback of this dataset over the Ganga-Brahmaputra basin dataset was the inclusion of the riverbed area into the built-up area, which leads to less accuracy in the damage assessment.

In the present study, the flooding vulnerability analysis is performed by identifying some of the elements at risk, which are defined by their level of exposure to the flood hazard. The elements at risk, such as the population, agricultural land, and urban areas, are identified with the help of the population datasets and LULC map. Future aspects of this research should consider flood hazards and risk through SAR-based data with the inclusion of the other characteristic features of the study area, such as elevation, slope, aspect, buildings, and infrastructure, which will help in disaster management. Hydrological models and DEM can be incorporated to determine the floodwater depth of the disaster. The available information about the depth of the floodwater and its hazardous impact on any area would be essential for disaster risk management. The SAR-derived flood inundation mapping together with the possible impact over the cropland and settlements and population would provide relevant information to the disaster management authority for a quick damage assessment and effective relief operations during flood impacts.

7. Conclusions

The present comprehensive study provides an insight into the utility of cloud platforms like GEE to process SAR data for mapping inundation over the Ganga-Brahmaputra basin. Without the cloud platform, it could have been impossible to map the flood characteristics over such a large area. The key findings can be summarized as floods have mostly occurred during July–September and, according to the composite flood maps over the Ganga-Brahmaputra basin, the maximum inundation extent was found in Bangladesh (25,889 km²) (18.5%), followed by Bihar (20,837 km²) (22.1%), West Bengal (17,307.1 km²) (20.3%), and Assam (13,460.1 km²) (17.1%), which are mainly driven by the high intensity rainfall in the upstream areas of the Ganga-Brahmaputra basin (i.e., Nepal, Arunachal Pradesh, and Nagaland), thereby causing riverine floods in the downstream areas that are mostly flat. The floods have caused inundation of up to 19.48% (77,493.1 km²) in the areas in the Ganga-Brahmaputra basin, which caused adverse impacts on agriculture (i.e., 23.68–28.47% of cropland area) as well as build-up (i.e., 5.66–9.15% of built-up area). Consequently, millions of the population were affected by the floods and the highest impact was seen in the Bihar state, as they reside in the lower valley and near the river. Similarly, the highest impacts were seen from Bangladesh because of the high population density as well as the settlement density.

The SAR data processing in the GEE platform and the derived flood extent map were very useful for large-scale flood mapping. The approaches of flood impact analysis and the information on the affected croplands and population can help disaster managers and policymakers to take flood mitigation measures and make a flood risk assessment in the susceptible zones of densely populated areas.

Author Contributions: A.C.P., K.K. and B.R.P.: Conceptualization, investigation, methodology, software, analysis, visualization, writing– original draft, review and editing. All authors have read and agreed to the published version of the manuscript.

Funding: This research received no external funding.

Institutional Review Board Statement: Not applicable.

Informed Consent Statement: Not applicable.

Data Availability Statement: Publicly available datasets were analyzed in this study. This data can be found from the source mentioned in Table 2. Code used for SAR-based flood mapping can be obtained from <https://www.un-spider.org> (accessed on 25 September 2021).

Conflicts of Interest: The authors declare no conflict of interest.

Appendix A

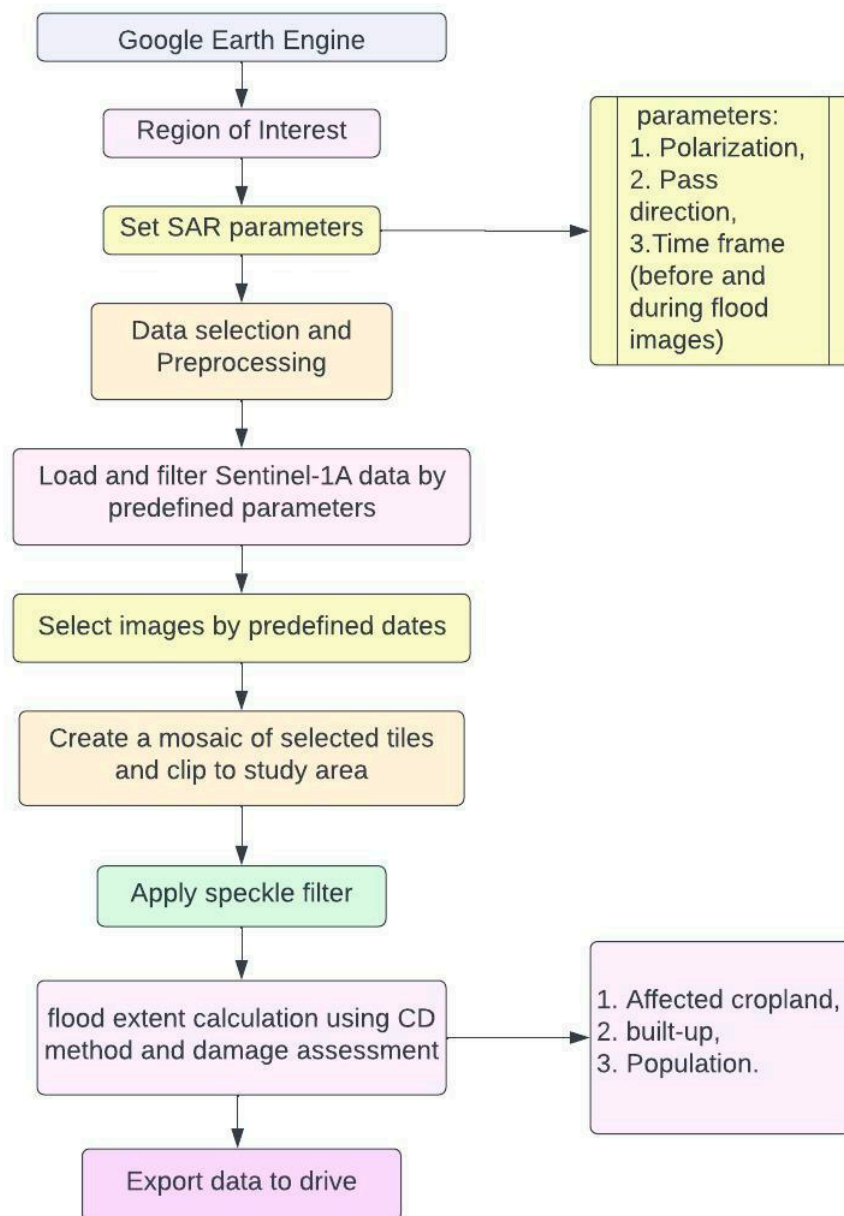


Figure A1. Flowchart showing steps carried out using GEE to deduce flood extent map.

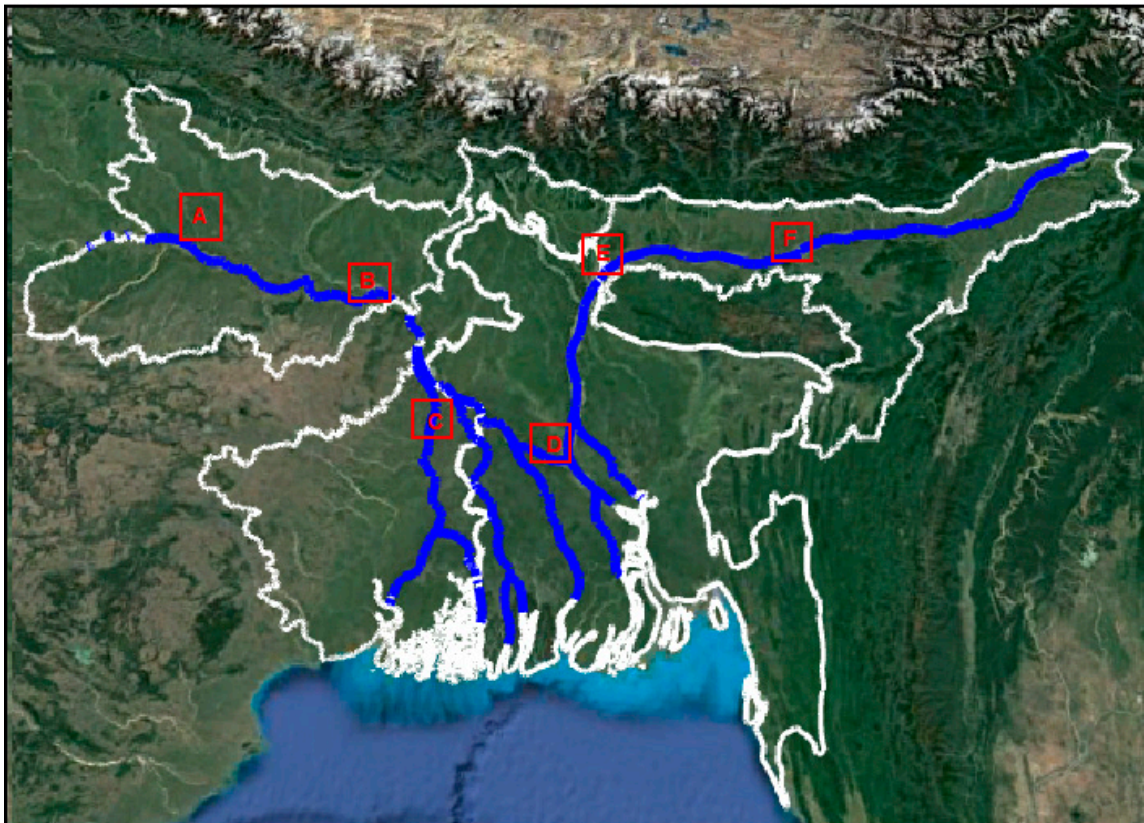
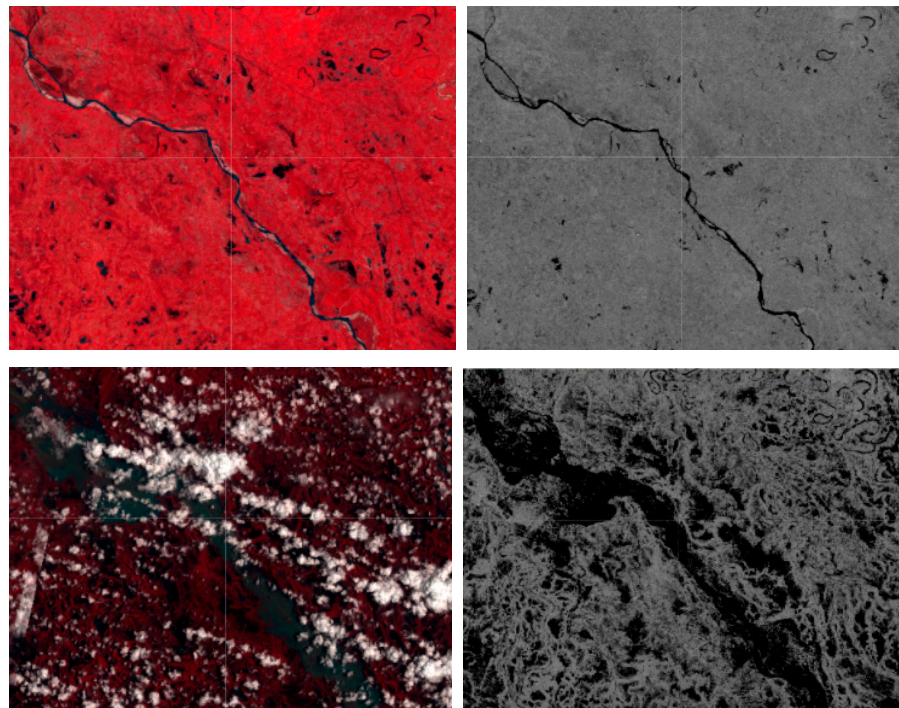
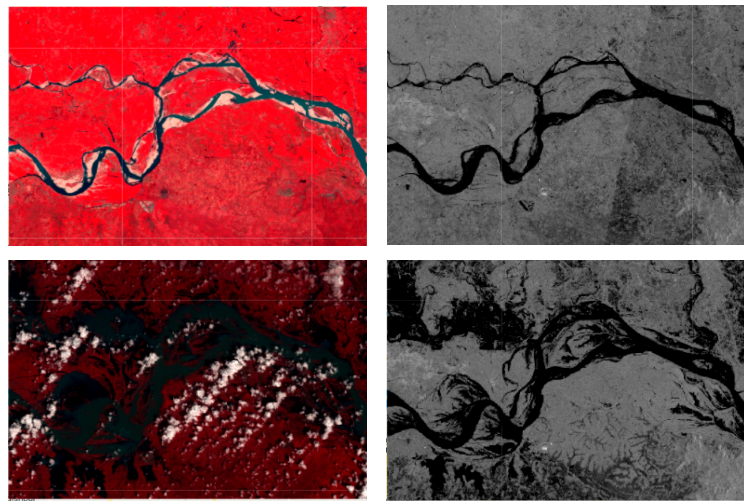


Figure A2. SAR-based flood extent validation using Landsat-8 images. The validation is shown for six subsets (A–F) across the study area as shown below.

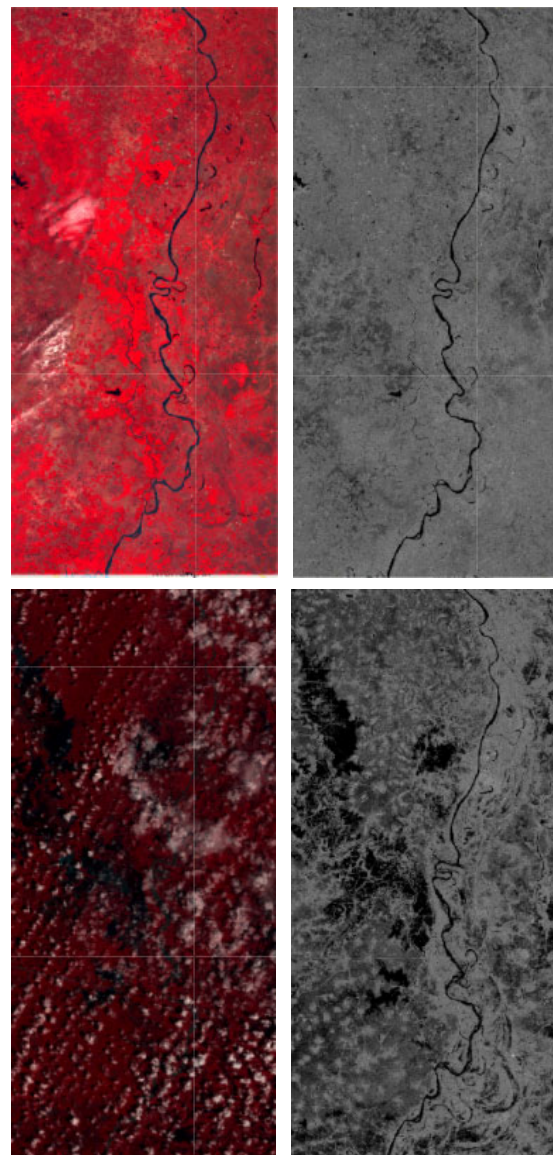


(A) Before (top) and during (bottom) flood images of Bihar (Optical and SAR)

Figure A3. *Cont.*

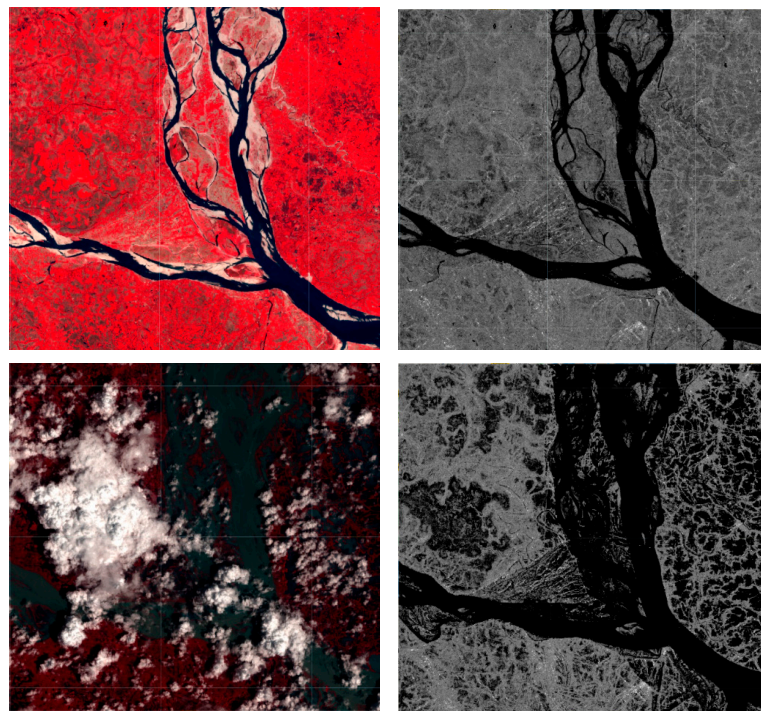


(B) Before (top) and during (bottom) flood images of Bihar

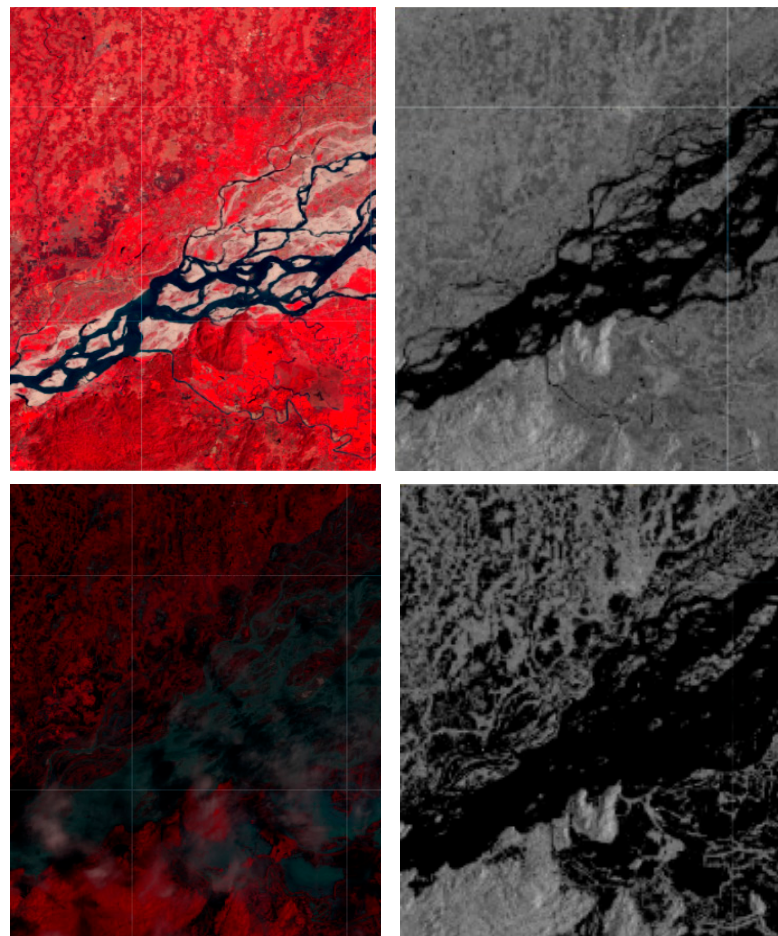


(C) Before (top) and during (bottom) flood images of West Bengal

Figure A3. Cont.

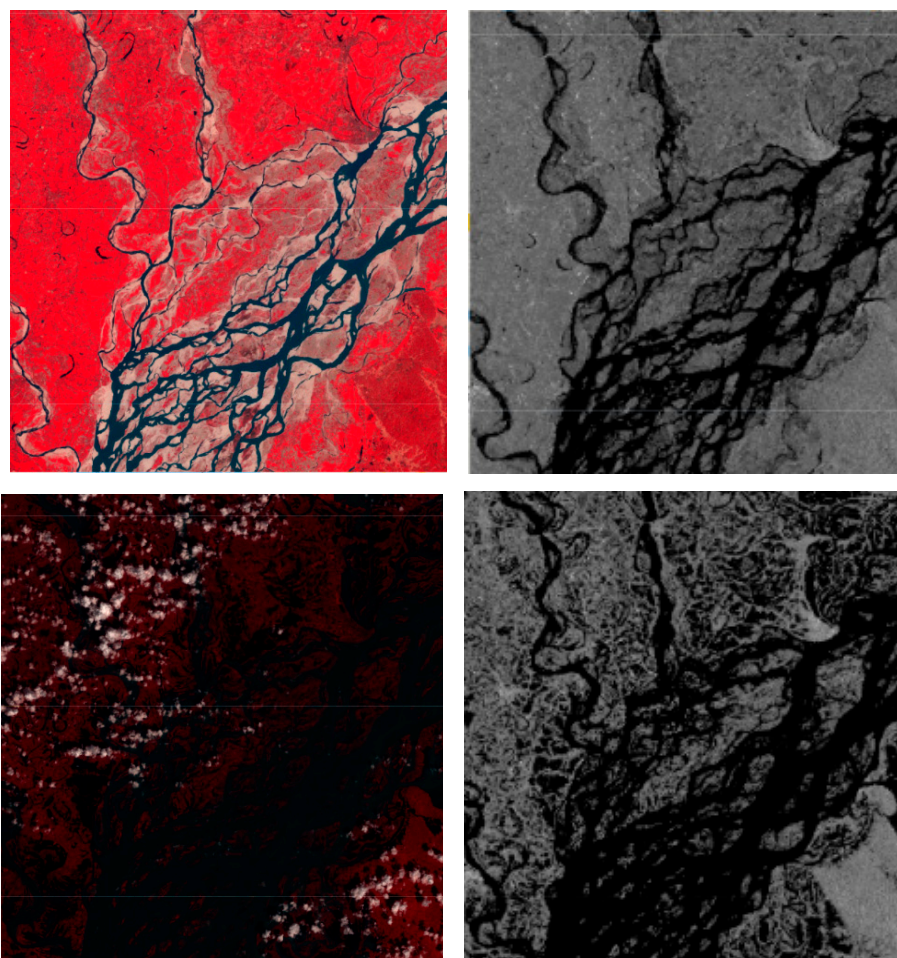


(D) Before (top) and during (bottom) flood images of Bangladesh



(E) Before (top) and during (bottom) flood images of Assam

Figure A3. Cont.



(F) Before (top) and during (bottom) flood images of Assam

Figure A3. (A)–(F) before and during flood images of optical and SAR at different location as shown in Figure A2.

References

1. Mirza, M.M.Q. Climate change, flooding in South Asia and implications. *Reg. Environ. Change* **2010**, *11*, 95–107. [[CrossRef](#)]
2. Gangopadhyay, P.K.; Sharma, B.R.; Pavelic, P. Co-solving Groundwater Depletion and Seasonal Flooding Through an Innovative Managed Aquifer Recharge Approach: Converting Pilot to a Regional Solution in the Ram Ganga Sub-basin. In *Clean and Sustainable Groundwater in India*; Springer: Berlin/Heidelberg, Germany, 2017; pp. 173–189.
3. Garg, P.K.; Garg, R.D. Geospatial techniques for flood inundation mapping. In Proceedings of the 2016 IEEE International Geoscience and Remote Sensing Symposium (IGARSS), Beijing, China, 10–15 July 2016; Institute of Electrical and Electronics Engineers (IEEE): Piscataway, NJ, USA, 2016; pp. 4387–4390.
4. Sahoo, S.N.; Sreeja, P. Development of Flood Inundation Maps and Quantification of Flood Risk in an Urban Catchment of Brahmaputra River. *ASCE-ASME J. Risk Uncertain. Eng. Syst. Part A Civ. Eng.* **2017**, *3*. [[CrossRef](#)]
5. Cohen, S.; Brakenridge, G.R.; Kettner, A.; Bates, B.; Nelson, J.; McDonald, R.; Huang, Y.-F.; Munasinghe, D.; Zhang, J. Estimating Floodwater Depths from Flood Inundation Maps and Topography. *JAWRA J. Am. Water Resour. Assoc.* **2017**, *54*, 847–858. [[CrossRef](#)]
6. Chutiya, D.; Hazarika, N.; Das, P. *Adjusting to Floods on the Brahmaputra Plains, Assam, India*; International Centre for Integrated Mountain Development (ICIMOD): Kathmandu, Nepal, 2009.
7. Wallemacq, P.; McClean, D. The Human Cost of Weather-Related Disasters 1995–2015. Technical Note 2015, 1–30. Available online: https://www.unisdr.org/files/46796_cop21weatherdisastersreport2015.pdf (accessed on 4 January 2022).
8. Luo, T.; Maddocks, A.; Iceland, C.; Ward, P.; Winsemius, H. World's 15 Countries with the Most People Exposed to River Floods. US-Based World Resources Institute (WRI). 2015. Available online: <https://www.wri.org/insights/worlds-15-countries-most-people-exposed-river-floods> (accessed on 21 December 2021).
9. Khan, S.; Sinha, R.; Whitehead, P.; Sarkar, S.; Jin, L.; Futter, M.N. Flows and sediment dynamics in the Ganga River under present and future climate scenarios. *Hydrol. Sci. J.* **2018**, *63*, 763–782. [[CrossRef](#)]

10. Rudra, K. Changing river courses in the western part of the Ganga–Brahmaputra delta. *Geomorphology* **2014**, *227*, 87–100. [[CrossRef](#)]
11. Milliman, J.D.; Farnsworth, K.L. *River Discharge to the Coastal Ocean*; Cambridge University Press: New York, NY, USA, 2011.
12. Kundzewicz, Z.; Kanae, S.; Seneviratne, S.; Handmer, J.; Nicholls, N.; Peduzzi, P.; Mechler, R.; Bouwer, L.M.; Arnell, N.; Mach, K.; et al. Flood risk and climate change: Global and regional perspectives. *Hydrol. Sci. J.* **2013**, *59*, 1–28. [[CrossRef](#)]
13. Immerzeel, W. Historical trends and future predictions of climate variability in the Brahmaputra basin. *Int. J. Clim.* **2007**, *28*, 243–254. [[CrossRef](#)]
14. Baruah, U.D.; Saikia, A.; Robeson, S.M.; Mili, N.; Chand, P. Perceptions and adaptation behavior of farmers to climate change in the upper Brahmaputra Valley, India. *Environ. Dev. Sustain.* **2021**, *23*, 15529–15549. [[CrossRef](#)]
15. Patel, A.; Goswami, A.; Dharpure, J.K.; Thamban, M. Rainfall variability over the Indus, Ganga, and Brahmaputra river basins: A spatio-temporal characterisation. *Quat. Int.* **2020**, 575–576, 280–294. [[CrossRef](#)]
16. Khalequzzaman Recent floods in Bangladesh: Possible causes and solutions. *Nat. Hazards* **1994**, *9*, 65–80. [[CrossRef](#)]
17. Kale, V.S. Geomorphic Effects of Monsoon Floods on Indian Rivers. *Nat. Hazards* **2003**, *28*, 65–84. [[CrossRef](#)]
18. Mirza, M.M.Q. Floods in Bangladesh: History, Dynamics and Rethinking the Role of the Himalayas. *Environ. Conserv.* **2007**, *34*, 348. [[CrossRef](#)]
19. Johnson, F.A.; Hutton, C.W. Dependence on agriculture and ecosystem services for livelihood in Northeast India and Bhutan: Vulnerability to climate change in the Tropical River Basins of the Upper Brahmaputra. *Clim. Chang.* **2012**, *127*, 107–121. [[CrossRef](#)]
20. Lal, P.; Prakash, A.; Kumar, A. Google Earth Engine for concurrent flood monitoring in the lower basin of Indo-Gangetic-Brahmaputra plains. *Nat. Hazards* **2020**, *104*, 1947–1952. [[CrossRef](#)]
21. Deka Rajib, L. Climate Change in the Brahmaputra Valley and Impact on Rice and Tea Productivity. Ph.D. Thesis, Centre for the Environment, Indian Institute of Technology, Guwahati, India, 2013.
22. Singh, R.B.; Pandey, B.W.; Prasad, A.S. Adaptation Strategies for Flood Risk Mitigation in Lower Brahmaputra River Basin, Assam through Integrated River Basin Management. *Trans. Inst. Indian Geogr.* **2014**, *36*, 159–170.
23. Ives, J.D. Deforestation in the Himalayas: The cause of increased flooding in Bangladesh and Northern India? *Land Use Policy* **1989**, *6*, 187–193. [[CrossRef](#)]
24. Islam, M.; Parvin, S.; Farukh, M. Impacts of riverbank erosion hazards in the Brahmaputra floodplain areas of Mymensingh in Bangladesh. *Progress. Agric.* **2017**, *28*, 73–83. [[CrossRef](#)]
25. Demir, V.; Kisi, O. Flood Hazard Mapping by Using Geographic Information System and Hydraulic Model: Mert River, Samsun, Turkey. *Adv. Meteorol.* **2016**, *2016*, 4891015. [[CrossRef](#)]
26. Jeyaseelan, A.T. Droughts & Floods Assessment and Monitoring Using Remote Sensing and GIS. In *Satellite Remote Sensing and GIS Applications in Agricultural Meteorology*; World Meteorological Organisation: Geneva, Switzerland, 2003; Available online: <http://www.wamis.org/agm/pubs/agm8/Paper-14.pdf> (accessed on 23 December 2021).
27. Amarnath, G. An algorithm for rapid flood inundation mapping from optical data using a reflectance differencing technique. *J. Flood Risk Manag.* **2013**, *7*, 239–250. [[CrossRef](#)]
28. Tiwari, V.; Kumar, V.; Matin, M.A.; Thapa, A.; Ellenburg, W.L.; Gupta, N.; Thapa, S. Flood inundation mapping- Kerala 2018; Harnessing the power of SAR, automatic threshold detection method and Google Earth Engine. *PLoS ONE* **2020**, *15*, e0237324. [[CrossRef](#)]
29. Cohen, S.; Raney, A.; Munasinghe, D.; Loftis, J.D.; Molthan, A.; Bell, J.; Rogers, L.; Galantowicz, J.; Brakenridge, G.R.; Kettner, A.J.; et al. The Floodwater Depth Estimation Tool (FwDET v2.0) for improved remote sensing analysis of coastal flooding. *Nat. Hazards Earth Syst. Sci.* **2019**, *19*, 2053–2065. [[CrossRef](#)]
30. Islam, A.S.; Bala, S.; Haque, M. Flood inundation map of Bangladesh using MODIS time-series images. *J. Flood Risk Manag.* **2010**, *3*, 210–222. [[CrossRef](#)]
31. Tripathi, G.; Pandey, A.C.; Parida, B.R.; Kumar, A. Flood Inundation Mapping and Impact Assessment Using Multi-Temporal Optical and SAR Satellite Data: A Case Study of 2017 Flood in Darbhanga District, Bihar, India. *Water Resour. Manag.* **2020**, *34*, 1871–1892. [[CrossRef](#)]
32. Huang, M.; Jin, S. Rapid Flood Mapping and Evaluation with a Supervised Classifier and Change Detection in Shouguang Using Sentinel-1 SAR and Sentinel-2 Optical Data. *Remote Sens.* **2020**, *12*, 2073. [[CrossRef](#)]
33. Patcoava, M.C.; Stancalie, G.; Raducanu, D. The Using of Satellite Image Data from Optic and Microwaves Data for Development of a Methodology for Identification and Extraction of Flooded Area. *Int. Arch. Photogramm. Remote Sens.* **2000**, *XXXIII*, 1185–1190.
34. Khan, S.I.; Hong, Y.; Wang, J.; Yilmaz, K.K.; Gourley, J.J.; Adler, R.F.; Brakenridge, G.R.; Policelli, F.; Habib, S.; Irwin, D. Satellite Remote Sensing and Hydrologic Modeling for Flood Inundation Mapping in Lake Victoria Basin: Implications for Hydrologic Prediction in Ungauged Basins. *IEEE Trans. Geosci. Remote Sens.* **2011**, *49*, 85–95. [[CrossRef](#)]
35. Matgen, P.; Hostache, R.; Schumann, G.; Pfister, L.; Hoffmann, L.; Savenije, H. Towards an automated SAR-based flood monitoring system: Lessons learned from two case studies. *Phys. Chem. Earth Parts A/B/C* **2011**, *36*, 241–252. [[CrossRef](#)]
36. Anusha, N.; Bharathi, B. Flood detection and flood mapping using multi-temporal synthetic aperture radar and optical data. *Egypt. J. Remote Sens. Space Sci.* **2019**, *23*, 207–219. [[CrossRef](#)]
37. Agnihotri, A.K.; Ohri, A.; Gaur, S.; Shivam; Das, N.; Mishra, S. Flood inundation mapping and monitoring using SAR data and its impact on Ramganga River in Ganga basin. *Environ. Monit. Assess.* **2019**, *191*, 760. [[CrossRef](#)]

38. Joyce, K.E.; Belliss, S.E.; Samsonov, S.V.; McNeill, S.J.; Glassey, P.J. A review of the status of satellite remote sensing and image processing techniques for mapping natural hazards and disasters. *Prog. Phys. Geogr. Earth Environ.* **2009**, *33*, 183–207. [CrossRef]
39. Parida, B.R.; Tripathi, G.; Pandey, A.C.; Kumar, A. Estimating floodwater depth using SAR-derived flood inundation maps and geomorphic model in kosi river basin (India). *Geocarto Int.* **2021**, 1–26. [CrossRef]
40. Tripathi, G.; Pandey, A.C.; Parida, B.R.; Shakya, A. Comparative Flood Inundation Mapping Utilizing Multi-Temporal Optical and SAR Satellite Data Over North Bihar Region: A Case Study of 2019 Flooding Event Over North Bihar. In *Spatial Information Science for Natural Resource Management*; IGI Global: Hershey, PA, USA, 2020; pp. 149–168. ISBN 978-1-79985-028-1.
41. Uddin, K.; Matin, M.A.; Meyer, F.J. Operational Flood Mapping Using Multi-Temporal Sentinel-1 SAR Images: A Case Study from Bangladesh. *Remote Sens.* **2019**, *11*, 1581. [CrossRef]
42. Gorelick, N.; Hancher, M.; Dixon, M.; Ilyushchenko, S.; Thau, D.; Moore, R. Google Earth Engine: Planetary-scale geospatial analysis for everyone. *Remote Sens. Environ.* **2017**, *202*, 18–27. [CrossRef]
43. ASDMA Assam State Disaster Management Plan. 2010, 1–195. Available online: <http://asdma.gov.in/pdf/asdmp.pdf> (accessed on 24 November 2021).
44. Water Resources by Government of Assam, India. Available online: <https://waterresources.assam.gov.in/> (accessed on 5 December 2021).
45. Samal, N.R.; Roy, P.K.; Majumadar, M.; Bhattacharya, S.; Biswasroy, M. Six Years Major Historical Urban Floods in West Bengal State in India: Comparative Analysis Using Neuro-Genetic Model. *Am. J. Water Resour.* **2014**, *2*, 41–53. [CrossRef]
46. Dewan, T.H. Societal impacts and vulnerability to floods in Bangladesh and Nepal. *Weather Clim. Extremes* **2014**, *7*, 36–42. [CrossRef]
47. Abatzoglou, J.T.; Dobrowski, S.; Parks, S.A.; Hegewisch, K.C. TerraClimate, a high-resolution global dataset of monthly climate and climatic water balance from 1958–2015. *Sci. Data* **2018**, *5*, 170191. [CrossRef]
48. Schiavina, M.; Freire, S.; MacManus, K. GHS-POP R2019A - GHS Population Grid Multitemporal (1975-1990-2000-2015). *Eur. Comm. Jt. Res. Cent.* **2019**. [CrossRef]
49. UN WPP-Adjusted Population Density, v4.11: Gridded Population of the World (GPW), v4; Center for International Earth Science Information Network—CIESIN—Columbia University: New York, NY, USA, 2018. [CrossRef]
50. Buchhorn, M.; Smets, B.; Bertels, L.; De Roo, B.; Lesiv, M.; Tsendbazar, N.-E.; Herold, M.; Fritz, S. Copernicus Global Land Service: Land Cover 100m: Collection 3: Epoch 2019: Globe. *OpenAIRE* **2020**. [CrossRef]
51. Conde, F.C.; Muñoz, M.D.M. Flood Monitoring Based on the Study of Sentinel-1 SAR Images: The Ebro River Case Study. *Water* **2019**, *11*, 2454. [CrossRef]
52. Martinis, S.; Rieke, C. Backscatter Analysis Using Multi-Temporal and Multi-Frequency SAR Data in the Context of Flood Mapping at River Saale, Germany. *Remote Sens.* **2015**, *7*, 7732–7752. [CrossRef]
53. Fan, J.; Sun, W.; Zhao, Y.; Xue, B.; Zuo, D.; Xu, Z. Trend Analyses of Extreme Precipitation Events in the Yarlung Zangbo River Basin, China Using a High-Resolution Precipitation Product. *Sustainability* **2018**, *10*, 1396. [CrossRef]
54. Loukas, A.; Garrote, L.; Vasiliades, L. Hydrological and Hydro-Meteorological Extremes and Related Risk and Uncertainty. *Water* **2021**, *13*, 377. [CrossRef]
55. Janes, T.; McGrath, F.; Macadam, I.; Jones, R. High-resolution climate projections for South Asia to inform climate impacts and adaptation studies in the Ganges-Brahmaputra-Meghna and Mahanadi deltas. *Sci. Total Environ.* **2018**, *650*, 1499–1520. [CrossRef] [PubMed]
56. Arshad, M.; Ma, X.; Yin, J.; Ullah, W.; Liu, M.; Ullah, I. Performance evaluation of ERA-5, JRA-55, MERRA-2, and CFS-2 reanalysis datasets, over diverse climate regions of Pakistan. *Weather Clim. Extremes* **2021**, *33*, 100373. [CrossRef]
57. Barman, S.; Bhattacharjya, R.K. Change in snow cover area of Brahmaputra river basin and its sensitivity to temperature. *Environ. Syst. Res.* **2015**, *4*, 16. [CrossRef]
58. Zhang, Y.; Xu, C.-Y.; Hao, Z.; Zhang, L.; Ju, Q.; Lai, X. Variation of Melt Water and Rainfall Runoff and Their Impacts on Streamflow Changes during Recent Decades in Two Tibetan Plateau Basins. *Water* **2020**, *12*, 3112. [CrossRef]
59. Yi, S.; Song, C.; Heki, K.; Kang, S.; Wang, Q.; Chang, L. Substantial Meltwater Contribution to the Brahmaputra Revealed by Satellite Gravimetry. *Cryosphere Discuss.* **2019**, *2*, 1–23. [CrossRef]
60. Tripathi, G.; Parida, B.R.; Pandey, A.C. Spatio-Temporal Rainfall Variability and Flood Prognosis Analysis Using Satellite Data over North Bihar during the August 2017 Flood Event. *Hydrology* **2019**, *6*, 38. [CrossRef]
61. Amarnath, G.; Matheswaran, K.; Pandey, P.; Alahacoon, N.; Yoshimoto, S. Flood Mapping Tools for Disaster Preparedness and Emergency Response Using Satellite Data and Hydrodynamic Models: A Case Study of Bagmati Basin, India. *Proc. Natl. Acad. Sci. India Sect. A Phys. Sci.* **2017**, *87*, 941–950. [CrossRef]
62. Tripathi, G.; Pandey, A.C.; Parida, B.R. Flood Hazard and Risk Zonation in North Bihar Using Satellite-Derived Historical Flood Events and Socio-Economic Data. *Sustainability* **2022**, *14*, 1472. [CrossRef]
63. Devrani, R.; Srivastava, P.; Kumar, R.; Kasana, P. Characterization and assessment of flood inundated areas of lower Brahmaputra River Basin using multitemporal Synthetic Aperture Radar data: A case study from NE India. *Geol. J.* **2021**, *57*, 622–646. [CrossRef]
64. Ghosh, S.; Dutta, S. Impact of climate change on flood characteristics in Brahmaputra basin using a macro-scale distributed hydrological model. *J. Earth Syst. Sci.* **2012**, *121*, 637–657. [CrossRef]
65. Modeling, F.; Sensing, R.; Images, S. Application of Remote Sensing and Gis for Flood Risk Analysis: A Case Study at Kalu-Ganga River, Sri Lanka. *Int. Arch. Photogramm. Remote Sens. Spat. Inf. Sci.* **2010**, XXXVIII, 110–115.

66. Freire, S.; MacManus, K.; Pesaresi, M.; Doxsey-Whitfield, E.; Mills, J. Development of New Open and Free Multi-Temporal Global Population Grids at 250 m Resolution. In Proceedings of the The 19th AGILE conference on Geographic Information Science, Helsinki, Finland, 14–17 June 2016.
67. Cutter, S.L.; Schumann, R.L.; Emrich, C.T. Exposure, Social Vulnerability and Recovery Disparities in New Jersey after Hurricane Sandy. *J. Extreme Events* **2014**, *1*, 1450002. [[CrossRef](#)]
68. Tate, E.; Rahman, A.; Emrich, C.T.; Sampson, C.C. Flood exposure and social vulnerability in the United States. *Nat. Hazards* **2021**, *106*, 435–457. [[CrossRef](#)]